Magnetic force microscopic study of $Ce_2(Fe, Co)_{14}B$, and its modifications by Ni and Cu

Tian Wang, Mamoun Medraj [*]

Department of Mechanical and Industrial Engineering, Concordia University, 1455 de Maisonneuve Boul. West, Montreal, QC H3G 1M8, Canada

ABSTRACT

The domain width and domain wall energy of the $Ce_2Fe_{14-x}Co_xB$ solid solution are studied for the first time in this work. The influence of Co content on these properties has been analyzed with the aid of magnetic force microscopy using diffusion couple and key alloys. The domain widths of $Ce_2Fe_{14-x}Co_xB$ decreased with increasing Co content at about 0.02 μm per 1 at.% Co. In $Ce_2Fe_{14-x}Co_xB$, phase shift, domain width and saturation magnetization are related in a way that lower average domain width is associated with higher phase shift and higher saturation magnetization. The highest domain wall energy of $Ce_2Fe_{14-x}Co_xB$ is measured as 31.7 erg/cm^2 after dissolving 14 at.% Co (x = 2.38). The effects of Ni and Cu on the domain width and domain wall energy of $Ce_2Fe_{14-x}Co_xB$ (x = 1.02) are also studied and reported using response surfaces. The domain width and domain wall energy of this solid solution increased after doping with 1 at.% Ni at constant Co content of 6 at.%, measuring 1.39 μm for domain width and 33.4 erg/cm^2 for domain wall energy. Both properties were determined as 0.71 μm and 18.6 erg/cm^2, respectively, after doping with 0.8 at.% Cu, while keeping Co content constant at 6 at.%. When $Ce_2Fe_{14-x}Co_xB$ (x = 1.02) is doped with both Ni (1 at.%) and Cu (0.8 at.%), the domain width and domain wall energy measured 0.99 μm and 33.8 erg/cm^2, respectively.

© 2018 Elsevier B.V. All rights reserved.

1. Introduction

Microstructural aspects have a strong influence on the magnetic coercivity and remanence. An important attribute in explaining the improvements in the magnetic properties is the magnetic domains morphology and interaction which depend on the domain size and domain wall energy [1]. Besides the main magnetic matrix phase, some minor phases are also required at the grain boundaries to pin the domain wall movement which could also affect the extrinsic magnetic properties [2]. For the bulk materials, only the magnetic structure near the surface of the samples can be investigated. Unlike thin films, where it is generally assumed that the observed domain boundary walls continue through the depth of the sample, it is more complicated to interpret the domain behavior in the interior of the bulk samples [3,5]. However, the MFM's tip stray field does not modify the magnetic state of bulk sample which could present a good approximation of the near surface magnetic structure [5]. Also, the domain structure evolved in thin films does not accurately represent the domain structure in

bulk materials which are suitable for permanent magnets [3]. Additionally, the magnetic properties of thin films were found changing with the annealing temperature, which makes it difficult to evaluate the relations between magnetic domain structure and magnetic property [6,7]. Hence, it is preferable to study domain structures of permanent magnet samples in bulk forms.

The intrinsic magnetic properties of $Ce_2Fe_{14-x}Co_xB$ have been reported in [4]. So far, there is a lack of magnetic domain structure investigations of $Ce_2Fe_{14-x}Co_xB$. Therefore, it is essential to interpret the domain structure of the $Ce_2Fe_{14-x}Co_xB$ and to determine the domain wall energy. In this study, the domain size has been measured combining magnetic force microscopy (MFM) with diffusion couple and key alloys. By applying MFM and diffusion couple, the influence of Co on the domain size variation of $Ce_2Fe_{14-x}Co_xB$ can be readily understood. Key alloys are designed to confirm the results obtained from the diffusion couple and to understand the magnetic domain morphology of $Ce_2Fe_{14-x}Co_xB$. Ni and Cu were reported to be beneficial to the magnetic properties of $Nd_2Fe_{14}B$ magnets, especially in improving the thermal stability [8–10]. However, limited literature data can be found regarding the effects of these additives on $Ce_2Fe_{14-x}Co_xB$. This paper also attempts to understand the effects of Ni and Cu on the domain size and domain wall energy of $Ce_2Fe_{14-x}Co_xB$.

* Corresponding author.
  E-mail address: mmedraj@encs.concordia.ca (M. Medraj).

2. Materials and methods

Pure elements with 99 wt.% purity or higher are used as the starting materials. All the elements are supplied by Alfa Aesar® (Haverhill, MA, USA). Samples of known composition are prepared from pure metals using an arc melting furnace under argon atmosphere. The arc melting furnace is equipped with a water-cooled copper crucible and a non-consumable tungsten electrode. Every alloy had to be melted several times to ensure homogeneity. The prepared samples were used as key alloys or as end-members for the diffusion-couple experiments. Diffusion couples were prepared by grinding down the contacting interfaces of end-members using 1200 grit SiC paper and then polished down to 1 μm using alcohol-based diamond suspension. 99% pure ethanol was used as lubricant. The selected end-members were carefully pressed and clamped together using a stainless steel ring. For the annealing process, samples were encapsulated inside quartz tubes under vacuum. After sufficient annealing time (at least 25 days), samples were quenched in a cold water bath to obtain the high-temperature structure. Quenched samples or diffusion couples were grinded and polished down to 1 μm in order to be analyzed using SEM coupled with Energy/Wavelength Dispersive X-ray Spectroscopes (EDS/WDS) and MFM. The microstructure and phase composition of the samples were analyzed by SEM/WDS (HITACHI S-3400 N, HITACHI, Tokyo, Japan). XRD was performed for the key alloys using PANAnalytical Xpert Pro X-ray diffractometer (PANAnalytical, Almelo, The Netherlands) with a CuK radiation at 45 kV and 35 mA. XRD patterns were analyzed using X'Pert Highscore plus software [11] and the Rietveld method. The crystal structure prototypes of the detected phases were obtained from Pearson's Database [12] and used in XRD analysis.

Saturation magnetization was measured using Quantum Design Physical Property Measurement System (PPMS-9 T, San Diego, CA, USA) at 298 K. The quenched samples were cut into cubic shape having around 30 mg weight. The saturation magnetization was obtained in external fields up to 50 kOe. Since Ce-Fe-Co-B is a complex multi-component system, it is extremely difficult to obtain single phase samples and because certain magnetic phases such as $Ce_2(Fe, Co)_{14}B$ form through a peritectic reaction [4], this makes it more difficult to obtain 100% single phase. To measure the saturation magnetization, over 80 wt.% of the magnetic phase with very limited impurities were obtained after annealing in all the samples. In order to precisely describe the saturation magnetization of the $Ce_2Fe_{14}B$ and its modifications, all the $M_s^{Ce2Fe14-xCoxB}$ results reported in this paper have been corrected based on the following equation:

$$M_s^{sample} = (w_i^{Ce2Fe14-xCoxB} \times M_s^{Ce2Fe14-xCoxB} + w_i^{imp} \times M_s^{imp})/100 \qquad (1)$$

where M_s^{sample} is the saturation magnetization of the sample obtained using PPMS; $w_i^{Ce2Fe14-xCoxB}$ and w_i^{imp} are the weight percentage of $Ce_2Fe_{14-x}Co_xB$ and impurity obtained using XRD through Rietveld analysis; M_s^{imp} is the saturation magnetization of the impurity taken from literature.

The magnetic domain structures of samples are investigated by Magnetic Force Microscopy (MFM) using Digital Instruments Multimode Atomic Force Microscope (Digital Instruments, Billerica, MA, USA) in LiftMode. In this work, a 225 μm long silicon cantilever having a magnetic pyramidal tip is used to acquire the magnetic force gradient distribution on the sample surface by oscillating the cantilever normal to the surface at its resonant frequency. The MFM tip, supplied by Appnano Ltd. (Mountain View, CA, USA), is coated with an approximately 50 nm CoCr layer. The magnetized MFM tip is perpendicular to the sample surface and points downward during the measurement.

When imaging with MFM, one concern is that stray fields from the magnetic tip modifies the micromagnetic structure of the sample [13]. A test for this is usually performed by observing the dependence of the micromagnetic structure on the MFM tip scan height [14]. For the samples studied in this work, there was no variation of the sample micromagnetic structure when the tip scan height was varied between 30 and 200 nm. Thus, we assume that modification of the micromagnetic structure of the samples by the tip is negligible.

3. Results and discussion

3.1. Domain morphology and domain size

In our recent paper [4], the solubility limits of Co in $Ce_2Fe_{14-x}Co_xB$ was measured as 28 at.% ($x = 4.76$) at 900 °C. In order to study the influence of Co content on the domain width (D_w) of $Ce_2Fe_{14-x}Co_xB$, MFM is applied to scan the diffusion layers of the diffusion couple. The chemical compositions across the diffusion layers and the corresponding phases that formed in the diffusion layers are listed in Table 1 and the microstructure is shown in Fig. 1.

The backscattered electron (BSE) image of the diffusion layers is presented in Fig. 1(a). Four layers formed after annealing at 900 °C for 25 days. The compositions of the formed phases were determined using WDS analysis. The grey phase in layer 1 is identified as $Ce_2(Fe, Co)_{14}B$ with variable Co content. A WDS compositional profile of $Ce_2(Fe, Co)_{14}B$ in the diffusion couple is shown in Fig. 1 (b). The quaternary solid solubility of $Ce_2Fe_{14}B$ is 22 at.% Co. And the $Ce_2(Fe, Co)_{14}B$ is in equilibrium with α-(Fe, Co). Ce(Co, Fe)$_4$B (light regions) and α-(Fe, Co) (dark regions) were found in layer 2. Layer 3 contains α-(Fe, Co), Ce(Co, Fe)$_4$B and $Ce_2(Co, Fe)_{17}$ phases. γ-(Fe, Co) and $Ce_2(Co, Fe)_{17}$ are found in layer 4. Details of phase equilibria in the Ce-Fe-Co-B system can be found in [4].

Four MFM images for $Ce_2Fe_{14-x}Co_xB$ with different Co content are shown in Fig. 2. The strength of the near-surface stray fields were observed. MFM tests were first applied on the interface between layers 1 and 2. Then the tip was moved around 40 μm towards layer 1 to capture the second image where the Co content

Table 1
Chemical compositions across the $Ce_{13}Fe_{80}B_7/Co_{90}Ce_{10}$ diffusion couple and the corresponding phases.

Layer	Composition (at.%)				Corresponding phase
	Ce	Fe	Co	B	
1	12	82–60	0–22	6	$Ce_2(Fe, Co)_{14}B$
	0	100–82	0–18	0	α-(Fe, Co)
2	15	27–17	42–52	16	Ce(Co, Fe)$_4$B
	0	82–37	18–63	0	α-(Fe, Co)
3	0	35–33	65–67	0	α-(Fe, Co)
	16	6–1	63–68	15	Ce(Co, Fe)$_4$B
	11	14	75	0	$Ce_2(Co, Fe)_{17}$
4	0	11–0	89–100	0	γ-(Fe, Co)
	11	14–0	75–89	0	$Ce_2(Co, Fe)_{17}$
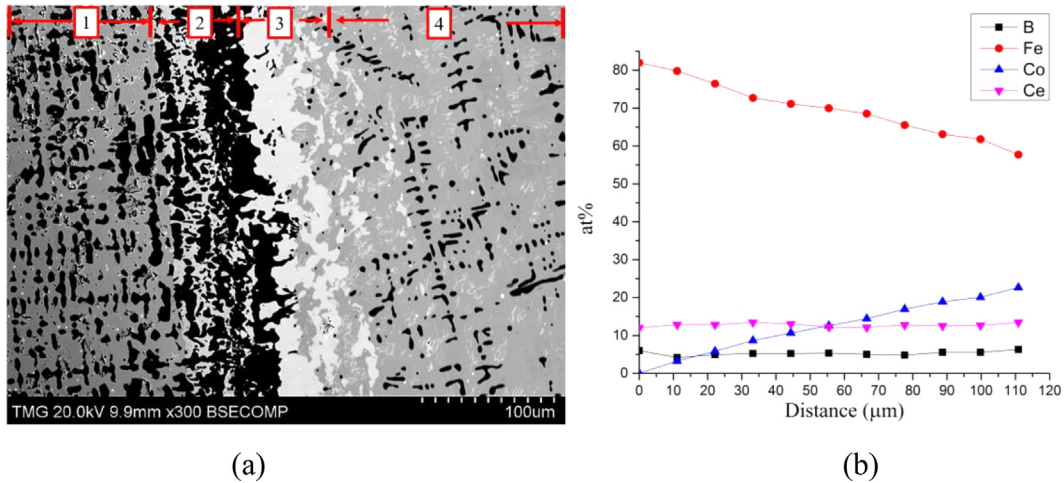
Fig. 1. (a) BSE image of $Ce_{13}Fe_{80}B_7/Co_{90}Ce_{10}$ diffusion couple; (b) WDS compositional profile of $Ce_2(Fe, Co)_{14}B$ in layer 1.
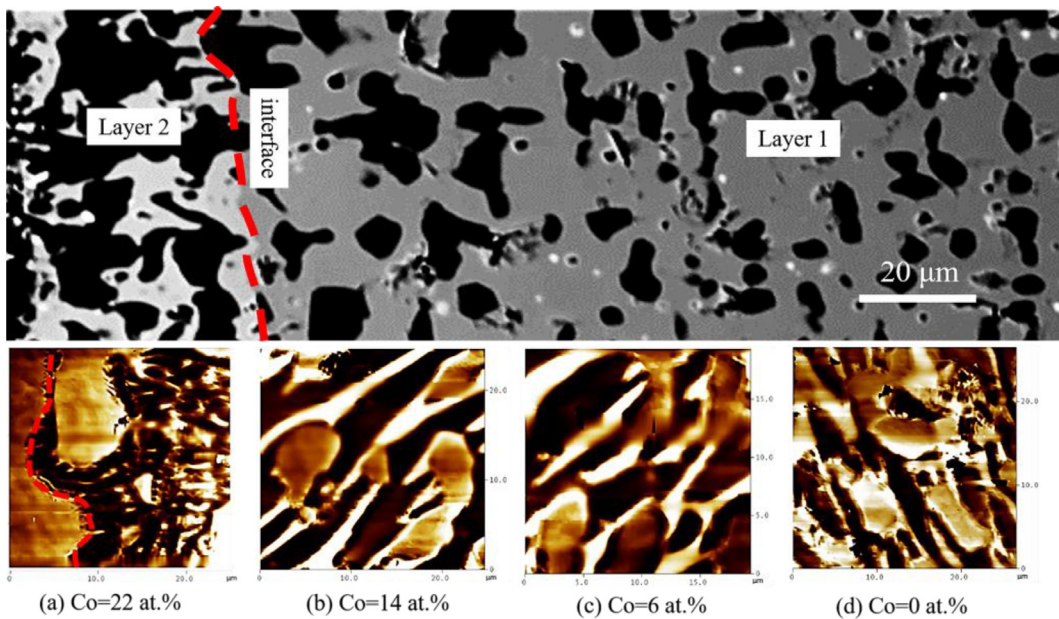

Fig. 2. Microstructure (top) and four MFM images (a-c) obtained from layer 1 to the interface with layer 2 of diffusion couple.

is around 14 at.% in $Ce_2Fe_{14-x}Co_xB$ ($x = 2.38$). Moving another 40 μm toward the edge of layer 1, the third MFM image was selected when Co content is about 6 at.%. The last MFM test was performed at the edge of layer 1 where negligible Co could be found in $Ce_2Fe_{14}B$.

The observed MFM contrast mechanism depends on the effective magnetic interaction gradient between the tip and the sample [2]. The dark image contrast indicates both the attractive interaction and the negative phase shift occur. Whereas, the positive phase shift and the bright image contrast result when repulsive interaction takes place [2]. During the MFM analysis, the phase shift ($(\Delta\Phi)_{rms}$) of the tip oscillation is directly proportional to the second derivative of the vertical component of the stray fields emerging from the surface of the sample [15]. Therefore, phase shift can give an indication of the effective magnetic moment of the sample such as the z-component of the stray field which is generally related to the saturation magnetization (M_s) [16]. Applying surface morphology analysis on these MFM images, the root mean square (RMS) values of phase shift are

measured, which can be used to represent the contrast of the magnetic force images. In general, for the MFM images with the same data scale, sharper color contrast corresponds to larger RMS values of phase shift $(\Delta\Phi)_{rms}$ [16]. Since the four MFM images from the diffusion couple were captured through the consecutive tests and testing conditions were maintained, the influence of Co content on the phase shift of $Ce_2Fe_{14-x}Co_xB$ could be interpreted which is presented in Fig. 3(a). The saturation magnetizations of $Ce_2Fe_{14-x}Co_xB$ at 6, 14 and 22 at.% Co ($x = 1.02, 2.38, 3.74$) are determined using key alloys and presented in this figure. It has been found that the phase shift and saturation magnetization all increase with the Co content in $Ce_2Fe_{14-x}Co_xB$. Also, by comparing the relations between phase shift and saturation magnetization of $Ce_2Fe_{14-x}Co_xB$ as shown in Fig. 3(b), they almost follow a linear trend where higher $(\Delta\Phi)_{rms}$ value corresponds to larger saturation magnetization of $Ce_2Fe_{14-x}Co_xB$. Therefore, determining $(\Delta\Phi)_{rms}$ values in the MFM analysis could be used as an assessment for the saturation magnetization of magnetic $Ce_2Fe_{14-x}Co_xB$ materials.
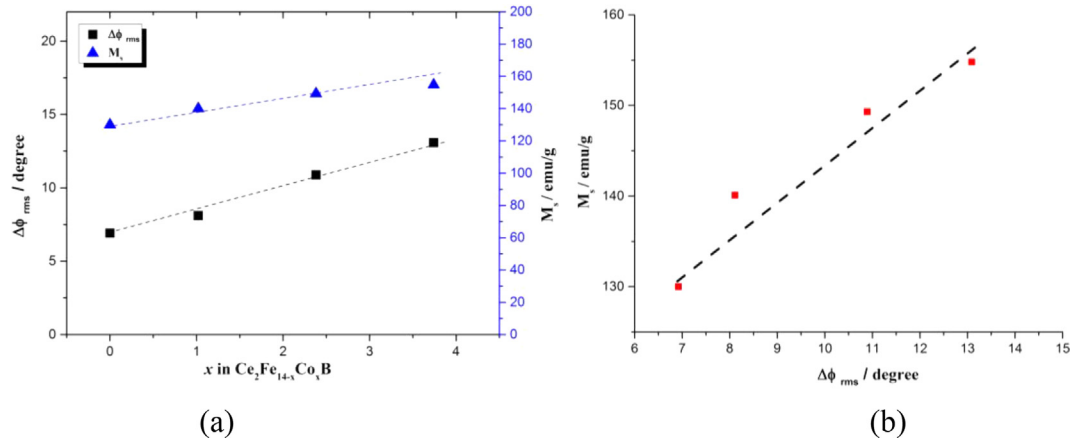
Fig. 3. (a) Phase shift and saturation magnetization of $Ce_2Fe_{14-x}Co_xB$ as a function of Co concentration; (b) saturation magnetization of $Ce_2Fe_{14-x}Co_xB$ as a function of phase shift.

Domain width measurement was carried out using the stereological method proposed in [2]. The effective domain width can be defined as the ratio between a test area and the total domain wall length in this area. The intersections of the domain walls with arbitrary test lines are counted and evaluated to calculate the effective domain width [2]. According to [2], the average domain width D_w is determined using the following equation:

$$D_w = \frac{2l}{\pi n} \qquad (2)$$

where l is the total length of the test lines and n is the number of intersections of the test lines with domain walls. The length of test line and the number of intersections can be obtained from section analysis, an example is shown in Fig. 4. The MFM images were enhanced via Nanoscope Analysis software [17] to remove the artifacts during the scans. Then, the clean image option was used to remove some streaks and noise which could affect the image interpretation. Sharpening process was done to enhance the contrast and provides a clearer image. Each image was subjected to 20 random direction test lines to cover all the test area. The measurements were repeated two times for each MFM image. The differences between the two tests were less than 0.03 μm.

The influence of Co content on the domain width of $Ce_2Fe_{14-x}Co_xB$, obtained using the diffusion couple, is summarized in Table 2. It can be seen that domain width of $Ce_2Fe_{14-x}Co_xB$

decreased with Co content at 0.02 μm per 1 at.%. Domain width could be related to the size of magnetic crystal [18]. By substituting different amount of Co, the volume of $Ce_2Fe_{14-x}Co_xB$ crystal decreased with Co content [4] as shown in Fig. 5. The domain width decreased correspondingly with Co content as can be seen in Table 2.

Four key alloys (KAs 1 to 4) were prepared to confirm the domain width results obtained from the diffusion couple and to study the domain structure as well as to measure the domain wall energy. $Ce_2Fe_{14-x}Co_xB$ at 6 at.% Co ($x = 1.02$) in KA 2 was reported to have the highest anisotropy field (H_a=29.3 kOe) in the $Ce_2Fe_{14-x}Co_xB$ ($0 \leq x \leq 4.76$) system [19]. Therefore to understand the effects of Ni and Cu on the domain width of $Ce_2Fe_{14-x}Co_xB$, KAs 5 to 7 were prepared and the Co content is kept the same (6 at.%) in order to be able to compare with KA 2. In KAs 5 and 6, about 1 at.% of Ni or Cu is added to replace Fe in the $Ce_2Fe_{14-x}Co_xB$ solid solution. Both Ni and Cu are added in KA 7 to compare the domain width variations with KAs 2, 5 and 6. After annealing at 900 °C for 25 days, dominating magnetic phases (over 80 wt.%) were obtained in all the samples with limited amount of impurities such as α-(Fe, Co). Based on the WDS analysis, α-(Fe, Co) was found to dissolve up to 20 at.% Co in KAs 1 to 4. The M_s of ferromagnetic α-(Fe, Co) at around 0, 10, 20, 30 at.% Co were reported in [20,21] as around 205 to 225 emu/g. The M_s of $Ce_2Fe_{14-x}Co_xB$ were then calculated following by the Eq. (1), as will be discussed
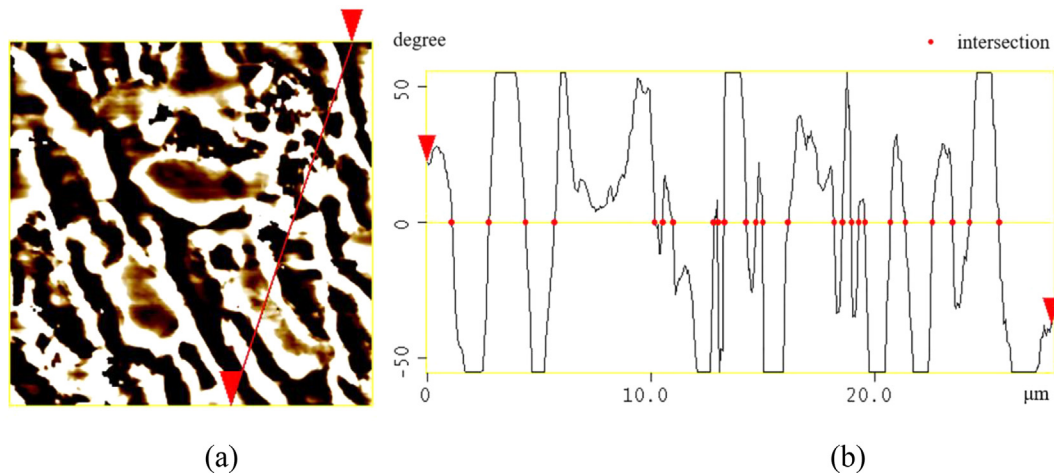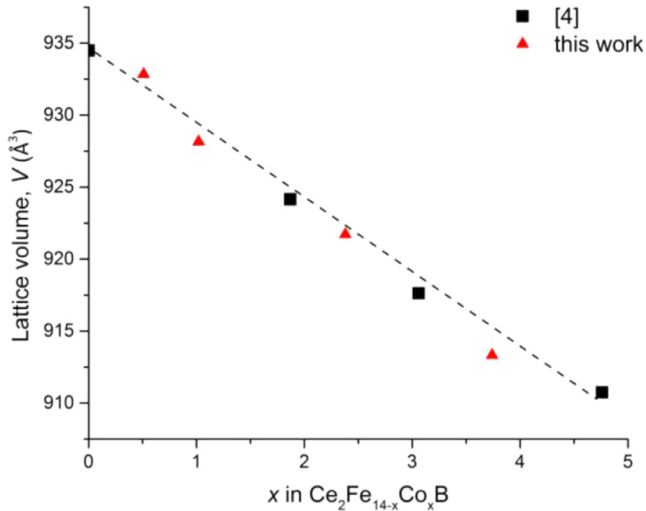

Fig. 4. (a) A random direction test line superimposed to apply section analysis; (b) section analysis results of the test line.

Table 2
Influence of Co content on average surface magnetic domain width of $Ce_2Fe_{14-x}Co_xB$.

x in $Ce_2Fe_{14-x}Co_xB$	D_w (μm)
0	1.19
1.02	1.03
2.38	0.98
3.74	0.79

Fig. 5. Lattice volume V of $Ce_2Fe_{14-x}Co_xB$ with x.

further below. The chemical compositions and domain widths of $Ce_2Fe_{14-x}Co_xB$ are listed in Table 3.

In this work, the dimensionless reduced anisotropy constant or magnet quality factor (Q) is calculated for $Ce_2Fe_{14}B$ as 7.8 based on Eq. (3) [23]:

$$Q = K_1/2\pi M_s^2 \qquad (3)$$

where K_1 is the first uniaxial magnetocrystalline anisotropy constant, which is reported to be 1.51×10^7 erg/cm^3 [22]; M_s is measured as 130 emu/g at 25 °C in this study. The domain structure of ferromagnets or ferrimagnets is a result of minimizing the total energy. In a ferromagnet, the total energy is the sum of different energy contributions such as exchange energy, magnetostatic energy, magnetocrystalline anisotropy energy, domain wall energy and magnetoelastic energy [24]. Certain flux closure domains at the sample's surface has to form to decrease the magnetostatic energy. As for strong uniaxial ferromagnets (with $Q \gg 1$), such magnets normally have large magnetocrystalline anisotropy energy which inhibits the formation of flux closure domains at the sample's surface. As such, the stray field leaks out of the sample and the associated energy cannot be eliminated entirely. However, in order to minimize energy, an appropriate geometrical arrangements of the

magnetic domains take place [23]. The magnetic domain structure is also related to the ratio between magnetocrystalline anisotropy energy and magnetostatic energy or stray field energy [23]. If the decrease in magnetostatic energy is greater than the energy needed to form magnetic domain walls, numerous surface magnetic domains will arise [23]. For the current uniaxial bulk polycrystalline samples which are in demagnetization state and the magnetic moments are randomly oriented, the magnetic domain structures may vary in different directions.

For example, two MFM tests have been first carried out on the top surface of KA 1 as shown in Fig. 6(a). The bulk wavy stripe domains indicate that the magnetic moments at the surface are either parallel or antiparallel to the easy axis and are separated by 180° domain walls. The magnetostatic interaction energy between the stripe domains and the tip is not perturbed resulting in nearly straight domain walls. The second test was done on the same sample but on the side cross section as shown in the Fig. 6(b). The 3D view of the domain structure of side cross section is shown in Fig. 6(c). The stripe like domain of $Ce_2Fe_{14-x}Co_xB$ in Fig. 6(a) turns into the matrix maze like domain in Fig. 6(b), indicating that the magnetization of $Ce_2Fe_{14-x}Co_xB$ crystal at the cross section is perpendicular or near-perpendicular to the alignment axis. There are some domains whose magnetization in the surface is perpendicular to the alignments appearing as spikes and reverse spikes domains visible as small white or dark spots in Fig. 6(c). This typical domain formed due to a compromise between magnetostatic energy and domain wall energy. They follow the domain walls which could reduce the domain wall energy and generate a strong surface anisotropy, also may reduce the density of magnetostatic energy near the surface [25,26]. The spike and reverse spike domains are associated with strong attractive and repulsive stray fields, respectively, which indicate high and low stray fields in the domain regions [26]. The MFM analysis on the top surface and side section of KA 1 is summarized by a schematic shown in Fig. 6(d). The c-axis is the magnetic easy axis and the branching bulk stripe domain of alternating interaction (attraction and repulsion) is revealed near the sample surface.

The enhanced MFM image of KA 1 with superimposed 20 random selected test lines is presented in Fig. 7. The domain widths of $Ce_2Fe_{14-x}Co_xB$ at Co = 3 at.% ($x = 0.51$) on the top surface and side cross section are similar and close to 1.14 μm. KAs 2 to 4 were used to determine the influence of Co content on the domain size of $Ce_2Fe_{14-x}Co_xB$. The average domain widths of $Ce_2Fe_{14-x}Co_xB$ in KAs 2 to 4 were measured as 1.01, 0.97 and 0.77 μm, respectively, which supports the results obtained from the diffusion couple, confirming that the domain width of $Ce_2Fe_{14-x}Co_xB$ reduces with increasing Co content.

According to the experimental results of [27], the domain width is proportional to the saturation magnetization. The average surface domain width of Nd-Fe-B increased by partial substitution of Dy for Nd, which leads to increased magnetic anisotropy field and domain wall energy γ [27]. However, the saturation magnetization M_s decreased with the Dy content [27]. Such relation between domain width and saturation magnetization also obtained through analyzing $Ce_2Fe_{14-x}Co_xB$ with different Co

Table 3
Chemical compositions and average domain widths of the dominating magnetic phase in the key alloys.

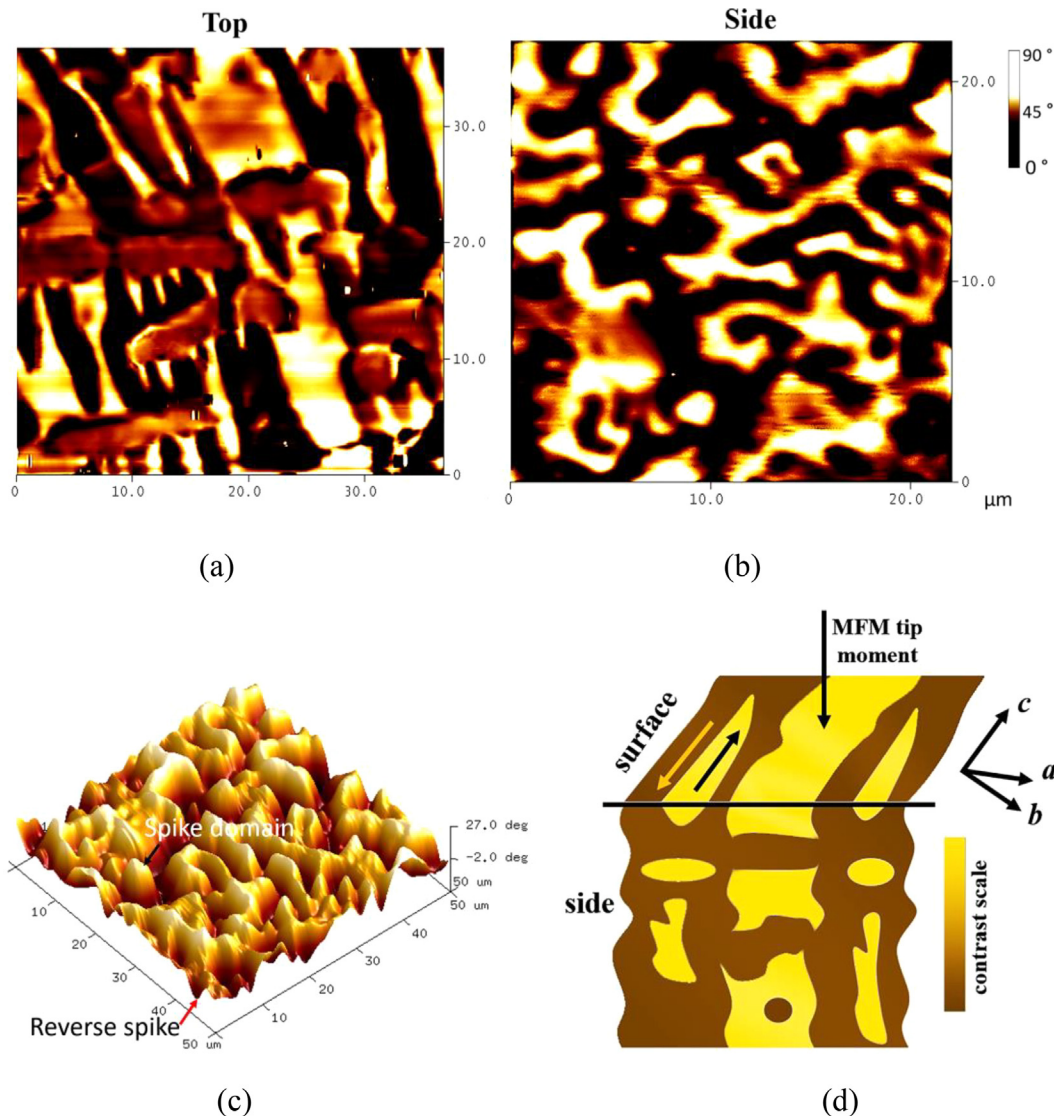| Key alloy	Dominating magnetic phase	at.%	x	y	z	D_w (μm)
KA 1	$Ce_2Fe_{14-x}Co_xB$	Co = 3	0.51	–	–	1.14
KA 2	$Ce_2Fe_{14-x}Co_xB$	Co = 6	1.02	–	–	1.01
KA 3	$Ce_2Fe_{14-x}Co_xB$	Co = 14	2.38	–	–	0.97
KA 4	$Ce_2Fe_{14-x}Co_xB$	Co = 22	3.74	–	–	0.77
KA 5	$Ce_2Fe_{14-x-y}Co_xNi_yB$	Co = 6; Ni = 1	1.02	0.17	–	1.39
KA 6	$Ce_2Fe_{14-x-z}Co_xCu_zB$	Co = 6; Cu = 0.8	1.02	-	0.136	0.71
KA 7	$Ce_2Fe_{14-x-y-z}Co_xNi_yCu_zB$	Co = 6; Ni = 1.2; Cu = 0.7	1.02	0.20	0.119	0.99

Fig. 6. (a) MFM image of (a) top surface of KA 1; (b) side cross section of KA 1; (c) 3D view of magnetic domain structure of side section of KA 1 (d) schematic of magnetic domain along the magnetization direction.

contents in this study. The average surface domain widths of $Ce_2Fe_{14-x}Co_xB$ as a function of x is shown in Fig. 8(a). It can be seen that the D_w reduces with Co content. By comparing the domain width and saturation magnetization of $Ce_2Fe_{14-x}Co_xB$ in Fig. 8(b), these two properties nearly follow a linear relation indicating that Co is effective in reducing the average domain width and improving the saturation magnetization of $Ce_2Fe_{14-x}Co_xB$. For $Ce_2Fe_{14-x}Co_xB$, the sample with smaller domain width has larger saturation magnetization, and higher phase shift in the MFM investigation.

The enhanced MFM images of KAs 5 to 7 are shown in Fig. 9. The average domain width of $Ce_2Fe_{12.98-y}Co_{1.02}Ni_yB$ ($y = 0.17$) is determined as 1.39 μm. In KA 6, the dominating $Ce_2Fe_{12.98-z}Co_{1.02}Cu_zB$ phase contained around 0.8 at.% Cu ($z = 0.136$) and 6 at.% Co. After applying the same measurement on the enhanced MFM image in Fig. 9(b), the average domain width of $Ce_2Fe_{12.98-z}Co_{1.02}Cu_zB$ ($z = 0.136$) is measured as 0.71 μm. The influence of adding both Ni and Cu on the domain width of $Ce_2Fe_{12.98-x}TM_xB$ (TM = Ni or Cu) is illustrated in Fig. 9(d). It can be concluded that a small amount of Ni, as low as 1 at.%, in $Ce_2Fe_{12.98-y}Co_{1.02}Ni_yB$ ($y = 0.17$) increases the domain width. Whereas, Cu reduces the domain width of Ce_2-$Fe_{12.98-z}Co_{1.02}Cu_zB$ ($z = 0.136$) at 6 at.% Co significantly. The domain

width of sintered $Nd_2Fe_{14}B$ is reported in [26] as 0.71 μm in the perpendicular direction to alignment direction and 1 μm in the parallel direction. Due to the influence of Ni, the domain width of $Ce_2Fe_{12.98-y}Co_{1.02}Ni_yB$ ($y = 0.17$) is greater than that of $Nd_2Fe_{14}B$. Ni and Ce atoms have large difference in electronegativity [28]. And substitutions of Ni for Fe will result in considerable electron transfer in the crystal, which could influence the exchange energy as well as the magnetic domain structure [29]. As can be seen in Fig. 9(a), the finer stripe domains indicate that the domain structure on grain surface are parallel to the easy direction. When both Ni and Cu are added, the domain width of $Ce_2Fe_{12.98-y-z}Co_{1.02}Ni_yCu_zB$ was determined as 0.99 μm when containing 1.2 at.% Ni ($y = 0.20$) and 0.7 at.% Cu ($z = 0.119$) at 6 at.% Co in KA 7, as shown in Fig. 9(c).

3.2. Domain wall energy

The domain wall energy is a fundamental magnetic parameter related to the coercivity, as it can be used as an approximation of the sum of the contributions from the exchange and magnetic anisotropy energies [27]. The knowledge of this parameter is also significant for understanding either nucleation or pinning is the
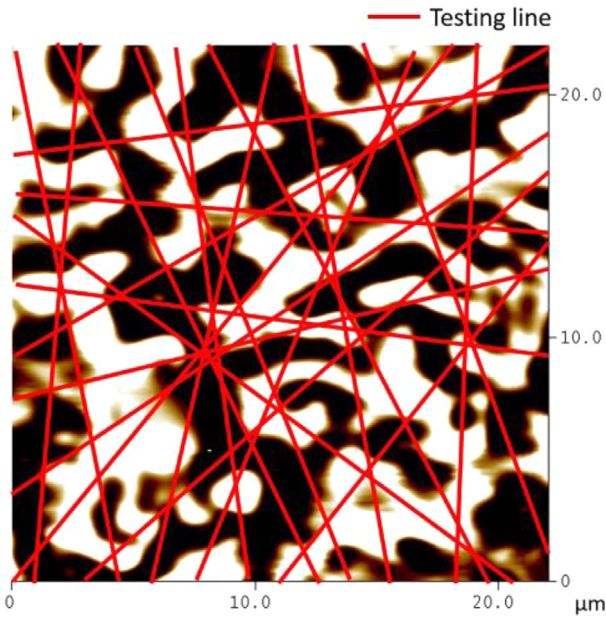
Fig. 7. Enhanced MFM image of KA 1.

dominant mechanism responsible for magnetic hardening [27]. The domain wall energy (γ_w) of $Ce_2Fe_{14}B$ as well as the magnetic phase in KAs 1 to 7 were calculated based on the following equation proposed by Bodenberger et al. [30]:

$$\gamma_w = \frac{D_w(M_s)^2}{4\pi\beta} \qquad (4)$$

where D_w is the average domain width and M_s is the saturation magnetization of the magnetic phase. β is a surface structure coefficient, and its value has been previously determined as 0.31 for $SmCo_5$ and similar magnetic materials with high magnetocrystalline anisotropy (for which the relative magnetic anisotropy $Q \gg 1$) [30]. Therefore, this value has been used in this work. The mass saturation magnetizations of $Ce_2Fe_{14}B$, $Ce_2Fe_{14-x}Co_xB$ in KAs 1 to 4, and $Ce_2Fe_{12.98-y-z}Co_{1.02}Ni_yCu_zB$ in KAs 5 to 7 were measured and converted into volume saturation magnetization using the density of $Ce_2Fe_{14}B$ as 7.56 g/cm³ reported in [31]. The calculation results are listed in Table 4.
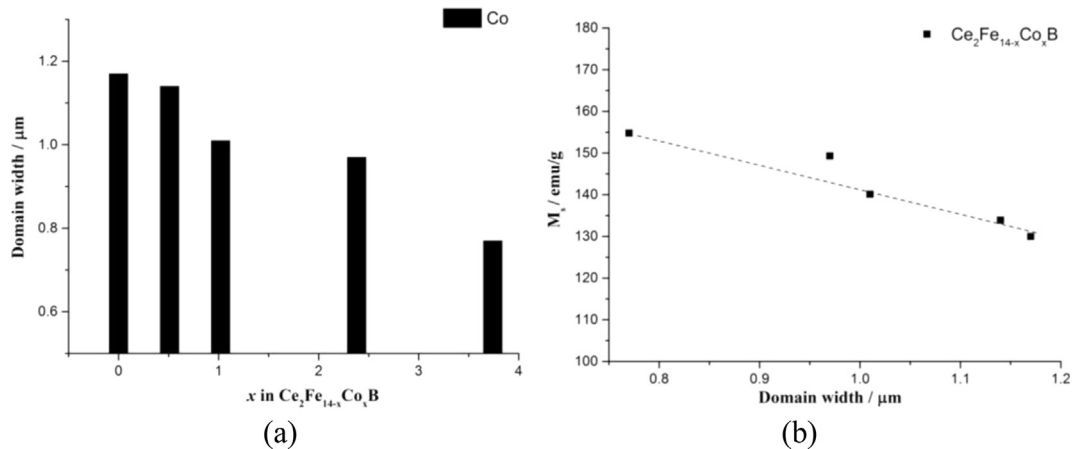
The domain wall energy of $Ce_2Fe_{14}B$ increased slightly from 29.0 to 30.0 erg/cm² after doping with 3 at.% Co and decreased back to 29.1 erg/cm² at 6 at.% Co. When containing 14 at.% Co, the domain wall energy of the solid solution increased reaching 31.7 erg/cm². Although both saturation magnetization of $Ce_2Fe_{11.62}Co_{2.38}B$ (14 at.% Co) and $Ce_2Fe_{10.26}Co_{3.74}B$ (22 at.% Co) are similar, γ_w of $Ce_2Fe_{10.26}Co_{3.74}B$ is still lower than that of $Ce_2Fe_{11.62}Co_{2.38}B$, because the average domain width in $Ce_2Fe_{10.26}Co_{3.74}B$ is 20% smaller than in $Ce_2Fe_{11.62}Co_{2.38}B$. Although the addition of Ni exhibited an improvement in domain wall energy, Cu reduced the domain wall energy significantly. The domain wall energy of $Ce_2Fe_{12.98-y}Co_{1.02}Ni_yB$ with 1 at.% Ni ($y = 0.17$) at 6 at.% Co was determined as 33.4 erg/cm². And the domain wall energy of $Ce_2Fe_{12.98-z}Co_{1.02}Cu_zB$ with 0.8 at.% Cu ($z = 0.136$) at 6 at.% Co was measured as 18.6 erg/cm². The highest domain wall energy of $Ce_2(Fe, Co)_{14}B$ was achieved as 33.8 erg/cm² when doping with 1.2 at.% Ni and 0.7 at.% Cu. Domain wall energy related to the domain wall thickness which is controlled by the short-range interactions between exchange energy and anisotropy energy [2]. Larger domain wall energy indicates that more domain walls are needed to split magnetic domains in the magnetic materials to minimize the magnetostatic energy of magnets [2]. Thus, the number of domain walls in KA 7 should be higher than KAs 2, 5 and 6. Based on the results obtained from KAs 2, 5, 6 and 7, the response surface plots of D_w and γ_w versus Ni and Cu content in $Ce_2Fe_{12.98-y-z}Co_{1.02}Ni_yCu_zB$ ($y \leq 0.20$, $z \leq 0.136$) at Co = 6 at.% are presented in Fig. 10. An appropriate response surface model could help understanding the relationship between several factors and the various magnetic properties. In summary, Ni substitution increases the domain width and the domain wall energy; whereas, Cu reduces the average domain width as well as domain wall energy in $Ce_2Fe_{12.98-z}Co_{1.02}Cu_zB$, which can be seen from Fig. 10. Also, it can be seen from this figure that Cu substitution does not affect the domain wall energy significantly at the higher level of Ni content.

Wyslocki et al. [1] used Eq. (4) to calculate the domain wall energy in $Y_2Fe_{13}MnB$ and $Y_2Fe_{12}Mn_3B$ as 22 erg/cm² and 3 erg/cm², respectively [1], which are lower than domain wall energy of Ce-Fe-Co-B type magnets. Yazid et al. [26] reported the domain wall energy of sintered Nd-Fe-B magnet as 38 erg/cm² and 26 erg/cm² in two different alignment directions. Bulk Ce-Fe-Co-B type magnets have similar domain width and domain wall energy as sintered Nd-Fe-B magnet. This indicates that Ce-Fe-Co-B magnets could be considered as a promising candidate for permanent magnets application. In addition, the extrinsic magnetic properties
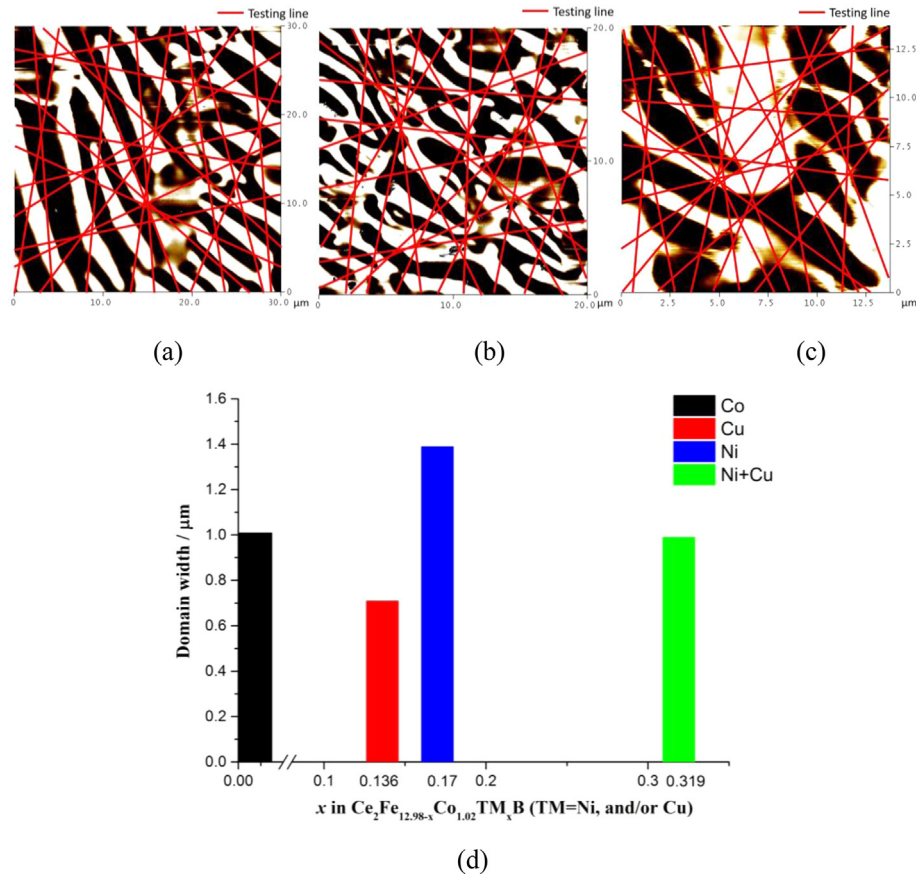

(a)

(b)

Fig. 8. (a) Average surface domain widths of $Ce_2Fe_{14-x}Co_xB$ as a function of Co content; and (b) domain width versus saturation magnetization of $Ce_2Fe_{14-x}Co_xB$.

(a)   (b)   (c)

(d)

Fig. 9. Enhanced MFM images of (a) KA 5; (b) KA 6; (c) KA 7; (d) domain width of $Ce_2Fe_{12.98-x}TM_xB$ (TM = Co, Ni or Cu) as a function of *x*.

Table 4
Domain wall energy.

Sample	M_s (emu/cm^3) at 25 °C	D_w (µm)	γ_w (erg/cm^2)
$Ce_2Fe_{14}B$	982.8	1.17	29.0
KA 1	1012.3	1.14	30.0
KA 2	1059.3	1.01	29.1
KA 3	1128.7	0.97	31.7
KA 4	1170.3	0.77	27.1
KA 5	967.7	1.39	33.4
KA 6	1010.1	0.71	18.6
KA 7	1153.7	0.99	33.8

(such as coercivity and remanence) can be measured to comprehend the influence of various additives on extrinsic magnetic properties of the Ce-Fe-Co-B magnets.

4. Conclusions

Combining magnetic force microscopy, diffusion couple and key alloys has been found to be effective in studying the magnetic domain structure, determining the domain width and calculating domain wall energy. The phase shift of $Ce_2Fe_{14-x}Co_xB$ increases with Co content which follows similar trend as its saturation magnetization. This indicates that higher phase shift in $Ce_2Fe_{14-x}Co_xB$ is
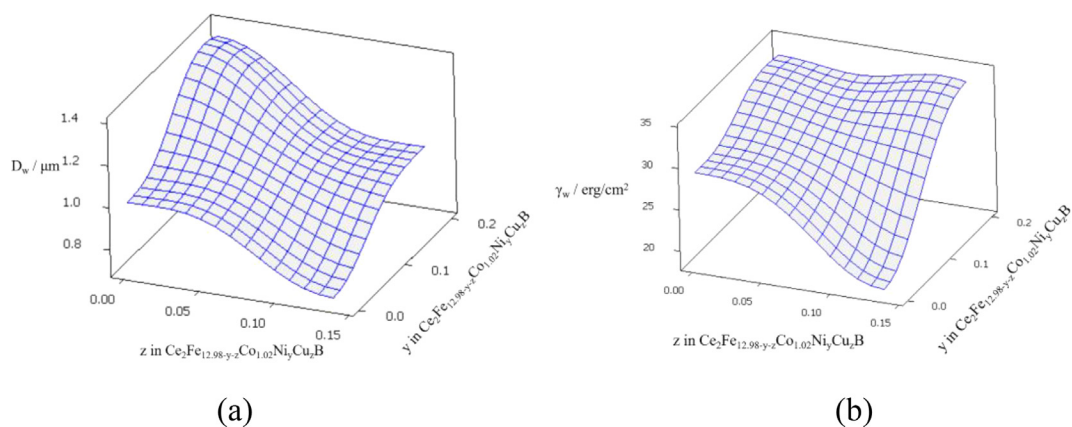

(a)   (b)

Fig. 10. Response surfaces of (a) D_w; (b) γ_w versus Cu and Ni contents in $Ce_2Fe_{12.98-y-z}Co_{1.02}Ni_yCu_zB$ at Co = 6 at.%.

associated with larger saturation magnetization. The domain width of $Ce_2Fe_{14-x}Co_xB$ dropped with increasing Co concentration at 0.02 µm per 1 at.% Co. Domain wall energy is related to the domain size and saturation magnetization. The highest domain wall energy of $Ce_2Fe_{14-x}Co_xB$ is found to be 31.7 erg/cm^2 after substituting 14 at. % Co ($x = 2.38$) for Fe. The influence of Ni and Cu on D_w and γ_w of $Ce_2Fe_{12.98-y-z}Co_{1.02}Ni_yCu_zB$ ($y \leq 0.20$, $z \leq 0.136$) at Co = 6 at.% are presented by the response surfaces. Ni is found to increase the domain width and domain wall energy of $Ce_2Fe_{12.98-y}Co_{1.02}Ni_yB$. While the domain width did not change significantly when both Ni and Cu are added, the domain wall energy was at maximum.

Acknowledgements

References

[1] J.J. Wysłocki, F. Bolzoni, Magnetic domain structure and domain-wall energy in $Y_2Fe_{13}MnB$ and $Y_2Fe_{12}Mn_3B$ compounds, J. Magn. Magn. Mater. 83 (1) (1990) 239–240.

[2] A. Hubert, R. Schafer, Magnetic Domains: The Analysis of Magnetic Microstructures, Springer-Verlag, Berlin Heidelberg, Germany, 1998, pp. 201–315.

[3] L. Folks, R.C. Woodward, The use of MFM for investigating domain structures in modern permanent magnet materials, J. Magn. Magn. Mater. 190 (1–2) (1998) 28–41.

[4] T. Wang, D. Kevorkov, M. Medraj, Phase equilibria and magnetic phases in the Ce-Fe-Co-B system, Materials 10 (1) (2017) 16.

[5] L. Batista, U. Rabe, S. Hirsekorn, Determination of the easy axes of small ferromagnetic precipitates in a bulk material by combined magnetic force microscopy and electron backscatter diffraction techniques, Ultramicroscopy 146 (2014) 17–46.

[6] B. Sun, G.Q. Li, W.X. Zhao, Z. Shen, Y.H. Liu, P. Chen, Perpendicular coercive force of thick CoFeB thin films grown on silicon substrate, Mater. Lett. 123 (2014) 221–223.

[7] C. Zhang, M. Yamanouchi, H. Sato, S. Fukami, S. Ikeda, F. Matsukura, H. Ohno, Magnetization reversal induced by in-plane current in Ta/CoFeB/MgO structures with perpendicular magnetic easy axis, J. Appl. Phys. 115 (2014) 17C714.

[8] C.D. Fuerst, E.G. Brewer, Diffusion alloyed additives in die upset Nd-Fe-B magnets, J. Appl. Phys. 69 (8) (1991) 5826–5828.

[9] F. Bolzoni, F. Leccabue, O. Moze, L. Pareti, M. Solzi, Magnetocrystalline anisotropy of Ni and Mn substituted $Nd_2Fe_{14}B$ compounds, J. Magn. Magn. Mater. 67 (3) (1987) 373–377.

[10] A.S. Kim, F.E. Camp, High performance NdFeB magnets (Invited), J. Appl. Phys. 79 (8) (1996) 5035–5039.

[11] X'Pert HighScore Plus, PANalytical B.V. Almelo, the Netherlands, Version: 2.2b (2.2.2), 2006.

[12] H. Putz, K. Brandenburg, Pearson's crystal data, crystal structure database for inorganic compounds, CD-ROM Software Version 1.3.

[13] U. Hartmann, Magnetic force microscopy: some remarks from the micromagnetic point of view, J. Appl. Phys. 64 (1988) 1561–1564.

[14] D. Rugar, H.J. Mamin, P. Guethner, S.E. Lambert, J.E. Stern, I. McFadyen, T. Yogi, Magnetic force microscopy: general principles and application to longitudinal recording media, J. Appl. Phys. 68 (3) (1990) 1169–1183.

[15] R.D. Gomez, E.R. Bruke, I.D. Mayergoyz, Magnetic imaging in the presence of external fields: technique and applications (invited), J. Appl. Phys. 79 (8) (1996) 6441–6446.

[16] X.A. Lin, C.J. Wei, T.L. Niu, W.F. Lin, Y. Zheng, H.B. Shan, Magnetic force microscopy study of alternate sputtered (001) oriented $L1_0$ phase FePt films, Chin. Phys. Lett. 24 (1) (2007) 222–225.

[17] Nanoscope Analysis, Bruker. Billerica, USA, Version: 1.4, 2011.

[18] I. Manke, N. Kardjilov, R. Schäfer, A. Hilger, M. Strobl, M. Dawson, C. Grünzweig, G. Behr, M. Hentschel, C. David, A. Kupsch, A. Lange, J. Banhart, Three-dimensional imaging of magnetic domains, Nat. Commun. 1 (2010) 125.

[19] T. Wang, M. Medraj, Intrinsic magnetic properties of $Ce_2(Fe, Co)_{14}B$ and modifications by Ni and Cu, J. Alloys Compd. to be submitted.

[20] I. Ohnuma, H. Enoki, O. Ikeda, R. Kainuma, H. Ohtani, B. Sundman, K. Ishida, Phase equilibria in the Fe-Co binary system, Acta Mater. 50 (2002) 379–393.

[21] F. Sánchez-De Jesús, A.M. Bolarín-Miró, C.A. Cortés Escobedo, G. Torres-Villaseñor, P. Vera-Serna, Structural analysis and magnetic properties of FeCo alloys obtained by mechanical alloying, J. Metall. 2016 (2016) 8347063.

[22] S. Hirosawa, Y. Matsuura, H. Yamamoto, S. Fujimura, M. Sagawa, H. Yamauchi, Single crystal measurements of anisotropy constants of $R_2Fe_{14}B$ (R=Y, Ce, Pr, Nd, Gd, Tb, Dy and Ho), Jpn. J. Appl. Phys. 24 (10) (1985) L803–L805.

[23] N. León-Brito, E.D. Bauer, F. Ronning, J.D. Thompson, R. Movshovich, Magnetic microstructure and magnetic properties of uniaxial itinerant ferromagnet Fe_3GeTe_2, J. Appl. Phys. 120 (2016) 080903–080908.

[24] W. Szmaja, Developments in the imaging of magnetic domains, Adv. Imag. Elect. Phys. 141 (2006) 175–256.

[25] M.A. Al-Khafaji, W.M. Rainforth, M.R.J. Gibbs, J.E.L. Bishop, H.A. Davies, The effect of tip type and scan height on magnetic domain images obtained by MFM, IEEE Trans. Magn. 32 (5) (1996) 4138–4140.

[26] M.M. Yazid, S.H. Olsen, G.J. Atkinson, MFM study of a sintered Nd-Fe-B magnet: Analyzing domain structure and measuring defect size in 3D view, IEEE Trans. Magn. 52 (6) (2017) 1–10.

[27] W. Szmaja, Investigations of the domain structure of anisotropic sintered Nd-Fe-B-based permanent magnets, J. Magn. Magn. Mater. 301 (2006) 546–561.

[28] A.R. Miedema, F.R. de Boer, R. Boom, Model predictions for the enthalpy of formation of transition metal alloys, Calphad 1 (1977) 341–359.

[29] M. Shimizu, J. Inoue, S. Nakagawa, Electronic structure and magnetic properties of Y-Ni intermetallic compounds, J. Phys. F: Met. Phys. 14 (1984) 2673–2687.

[30] R. Bodenberger, A. Hubert, Zur bestimmung der blochwandenergie von einachsigen ferromagneten, Phys. Status Solidi A. 44 (1) (1977) K7–K11.

[31] J.F. Herbst, $R_2Fe_{14}B$ materials: Intrinsic properties and technological aspects, Rev. Mod. Phys. 63 (1991) 819–898.